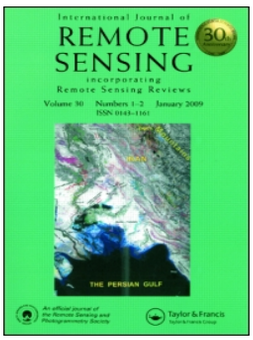

International Journal of Remote Sensing

ISSN: 0143-1161 (Print) 1366-5901 (Online) Journal homepage: http://www.tandfonline.com/loi/tres20

Radiometric calibration stability assessment for the RISAT-1 SAR sensor using a deployed point target array at the Desalpar site, Rann of Kutch, India

Shweta Sharma, Gautam Dadhich, Mihir Rambhia, Aloke K. Mathur, R.P Prajapati, P.R Patel & Alpana Shukla

To cite this article: Shweta Sharma, Gautam Dadhich, Mihir Rambhia, Aloke K. Mathur, R.P Prajapati, P.R Patel & Alpana Shukla (2017) Radiometric calibration stability assessment for the RISAT-1 SAR sensor using a deployed point target array at the Desalpar site, Rann of Kutch, India, International Journal of Remote Sensing, 38:23, 7242-7259

To link to this article: http://dx.doi.org/10.1080/01431161.2017.1371858

Published online: 03 Sep 2017.

INTERNATIONAL JOURNAL OF REMOTE SENSING, 2017
VOL. 38, NO. 23, 7242–7259
https://doi.org/10.1080/01431161.2017.1371858

Taylor & Francis
Taylor & Francis Group

Radiometric calibration stability assessment for the RISAT-1 SAR sensor using a deployed point target array at the Desalpar site, Rann of Kutch, India

Shweta Sharma[a], Gautam Dadhich[b], Mihir Rambhia[c], Aloke K. Mathur[a], R.P Prajapati[a], P.R Patel[b] and Alpana Shukla[c]

[a]Space Applications Centre, ISRO, Ahmedabad, India; [b]Nirma University of Science and Technology, Civil Engineering Department, Ahmedabad, India; [c]M.G. Science Institute, Department of Botany, Ahmedabad, India

ABSTRACT

Synthetic aperture radar (SAR) data used for quantitative temporal and/or spatial analysis requires calibration to ensure that observed pixel values of amplitude and phase can be related to the geophysical parameters of interest. The process of radiometric calibration of SAR images involves comparison of the backscattered radar reflectivity signal from a ground resolution element containing a calibration target of known signal response, such as a corner reflector. In this study, absolute radiometric calibration of RISAT-1 intensity data of fine resolution stripmap-1 (FRS-1) and medium resolution ScanSAR (MRS) mode was carried out by utilizing array of standard point targets of various types (triangular trihedral, square trihedral, and dihedral) with known radar cross-section deployed prior to satellite overpass with precise azimuth and elevation angles in Desalpar, Rann of Kutch in western India. The derived calibration constants using the integral method were then compared with the values provided in the header file. Deviations in the results are reported in this article. The results obtained show that the difference between the estimated average calibration constants for FRS-1 and MRS mode data with the provided value was found to be within the absolute radiometric accuracy specification of Radar Imaging SATellite (RISAT-1). Near-range to far-range difference of 0.1–0.2 dB for HH (Horizontal transmit, Horizontal receive) polarization and 0.1–0.3 dB for HV (Horizontal transmit, Vertical receive) polarization was estimated for the same scene using distributed target analysis indicating the stability of calibration for the same scene. This study also concluded that Desalpar site in Rann of Kutch has the potential of being an operational SAR calibration site.

ARTICLE HISTORY
Received 16 June 2016
Accepted 19 August 2017

1. Introduction

Radar Imaging SATellite (RISAT-1) is India's first indigenously developed space-borne C-band synthetic aperture radar (SAR) sensor satellite launched in 26 April 2012, and the

CONTACT Shweta Sharma shweta@sac.isro.gov.in Space Applications Centre, ISRO, Ahmedabad, India.
This work is supported by our own organization Space Applications Centre, ISRO, Ahmedabad.

operational phase of the mission started in the month of May 2012. RISAT-1 is not only capable of acquiring data in multi-polarization mode and quad linear polarization, but it is also first of its kind to operate in hybrid circular polarimetric mode for Earth observation (Misra et al. 2013; Misra and Kirankumar 2014). The specifications of RISAT-1 SAR sensor have been shown in Table 1 (Misra et al. 2013).

From the early stages of the mission, data quality of all data RISAT-1 data products are monitored routinely for radiometric calibration performance (Misra and Kirankumar 2014; Gupta, Kartikeyan, and Chowdhury 2014). SAR data used for temporal or spatial analysis need calibration to confirm that perceived pixel values of amplitude and phase can be related for retrieving the geophysical parameters (Dobson et al. 1986; Freeman 1992). In radiometric calibration, analysis of backscattered radar reflectivity signal of point target of known reflectivity is carried out (Gray et al. 1990; Corr 1982). Accurate backscatter estimates enable more robust use of the retrieved values in applications such as the monitoring of deforestation, land-cover classification, and delineation of wet snow-covered area. These backscattering coefficients rely completely on the calibration constant provided with the image data. To achieve calibration accuracies required for most scientific analysis, a complex process utilizing internal (built-in device) measurements and external (ground deployed device) measurements (Dobson et al. 1986; Freeman 1995;

Table 1. RISAT-1 beam modes and specifications.

	Polarization				
	Single pol	Dual pol	Circular (hybrid) pol	Quad pol	
Image quality mode	HH/HV/VV/VH	HH+HV/VV+VH	Rx: V and H	HH+HV+VV+VH	NESZ
High resolution spotlight mode (HRS)	1 m (azimuth) × 0.67 m (range) resolution 10 km ×10 km (10 km ×100 km experimental) spot Min σ_0 = −16 dB				−16 dB
Fine resolution stripmap mode-1 (FRS-1)	3 m (azimuth) × 2 m (range) resolution 25 km swath Min σ_0 = −17 dB				−17 dB
Fine resolution stripmap mode-II (FRS-II)			3 m (azimuth) × 4 m (range) resolution 25 km swath Min σ_0 = −19 dB	9 m (azimuth) × 4 m (range) resolution 25 km swath Min σ_0 = −20 dB	−19 dB (circular polarization) −20 dB (Quad Pol.)
Medium resolution ScanSAR mode (MRS)	21–23 m (azimuth) × 8 m (range) resolution 115 km swath Min σ_0 = −17 dB				−17 dB
Coarse resolution ScanSAR mode (CRS)	41–55 m (azimuth) × 8 m (range) resolution 223 km swath Min σ_0 = −17 dB				−17 dB

Swath coverage: Selectable within 107–659 km off-nadir distance on either side.
Incidence angle range: 12–55°.

Srivastava et al. 1996; Srivastava et al. 2003; Cote *et al.* 2007; Shimada et al. 2009; Touzi 2012; Shimada 2015) is needed. The external calibration technique generally involves two types of targets: point targets, for example, active target – active radar calibrator (transponder), passive targets – corner reflector (CR) (dihedral or trihedral), flat rectangular plate, sphere (metal), Luneberg – lens reflector, so on, and distributed targets, for example, Amazonian Rainforest (Freeman 1995; Srivastava et al. 1996).

Globally, various space-borne C-band sensors like ERS-1/2, ENVISAT, RADARSAT-1/2, and recently launched Sentinel-1A are available. For the calibration of these SAR sensors, various standard point targets viz. active and passive standard targets have been used in the past (Freeman 1995; Srivastava et al. 2001; Shimada et al. 2009; Touzi 2012; Shimada 2015; Schmidt et al. 2015; European Space Agency (ESA) 2015). In this study, passive standard targets (dihedral CR, triangular trihedral CR, and square triangular CR) have been utilized for RISAT-1 SAR calibration. Calibration constant for RISAT-1 data (both medium resolution ScanSAR (MRS) and fine resolution Stripmap-1 (FRS-1) mode data) has been derived using point target array, deployed synchronous to satellite pass, and then the estimated constants were compared with the provided values in order to assess the radiometric calibration stability of RISAT-1 data. The major objective of the study is to assess the radiometric calibration stability of FRS-1 and MRS mode intensity data of SAR sensor on board RISAT-1 satellite using point target array deployment in Desalpar, Rann of Kutch, western India. For CRs' response analysis, co-polarization and circular polarization images, i.e. HH (horizontal transmit, horizontal receive), RH (right hand circularly polarized transmit and linearly receive in horizontal polarization), and RV (right hand circularly polarized transmit and linearly receive in vertical polarization) were used in the present study. Near and far range calibration stability was also studied using three scenes (16 January 2014, 23 February 2014, and 17 February 2015) of Amazon rainforest MRS data of HH and HV polarization (horizontal transmit, vertical receive). The stability of only radiometric calibration of dual polarization (HH–HV) and compact (RH–RV) polarization data has been assessed. Calibration of polarimetric mode will be considered in a future paper.

2. Study area and data used

2.1. *Study site*

The selection of suitable site for the deployment of standard point targets is the major requirement for proper calibration of the data. Flatness and homogeneity of the surrounding land, devoid of vegetation, metallic boundary fences, perceived sources of radar clutter, and large area in order to avoid overlap of adjacent point target (CRs) responses are the factors that are taken into account when choosing sites for point target deployment.

Based on the abovementioned factors, for the present study, Desalpar, Rann of Kutch site (with Latitude 23°46′14.10″N and Longitude 70°43′19.30″E) was selected for point target deployment (Figure 1). The size of this site is 3 km × 7 km. Figure 1 shows the location of the study area in false colour composite (FCC) image of Resourcesat-2 LISS-4 sensor having green, red, and NIR bands.

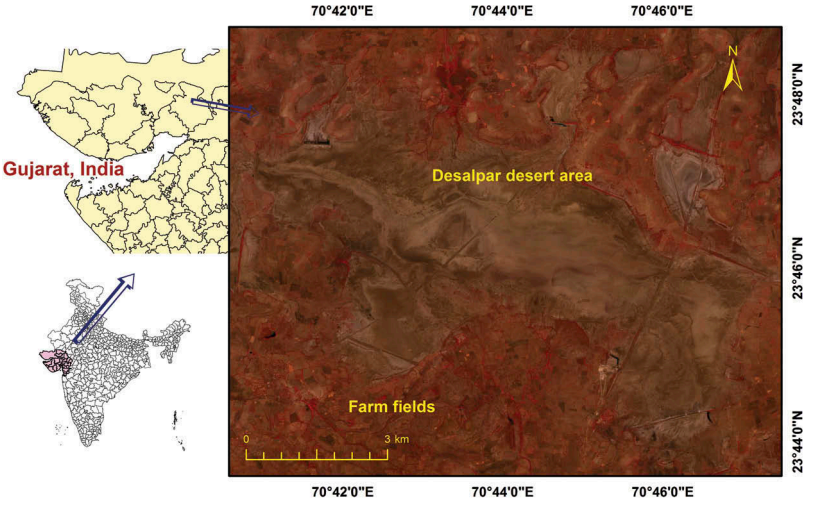

Figure 1. Map showing the location of study area (Desalpar Cal Val site) within Gujarat, India, in FCC image of Resoursesat-2 LISS-4 sensor.

This site is an extensive mudflat which gets inundated during monsoon and flooding from fresh inland and saline water from the Gulf of Kutch during June–August. During summer months (March–July), the Rann becomes dry and barren with high temperatures (>40°C), resulting in creation of salt-encrusted flat wasteland, totally devoid of vegetation. The fact that the site is devoid of buildings and vegetation and its large uniform area makes this site a potential site for the calibration of high and medium resolution SAR sensors.

2.2. *Data used*

RISAT-1 intensity images of FRS-1 and MRS mode with various types of polarization were acquired over the area of interest during January 2016–March 2016. Details of the data used in the study are shown in Table 2.

2.3. *Types of* CRs *used*

For the study, various types of CRs were used. Figure 2 shows the triangular trihedral (inner leg length of 90 cm), square trihedral (inner leg length of 60 cm), and dihedral

Table 2. Details of the RISAT-1 data used in the study.

Mode	Date	Polarization	Beam no.	Incidence angle (°)	Node	Orientation
FRS-1 SLC	22 January 2016	RH, RV	66	14	Ascending	Left
FRS-1 SLC	15 February 2016	RH, RV	87	32	Ascending	Right
FRS-1 SLC and GRD	10 March 2016	RH, RV	107	46	Ascending	Left
FRS-1 SLC and GRD	11 March 2016	RH, RV	87	32	Ascending	Right
MRS GRD	14 February 2016	HH, HV	87–97	36	Descending	Left
MRS GRD	10 March 2016	HH, HV	87–97	36	Descending	Left

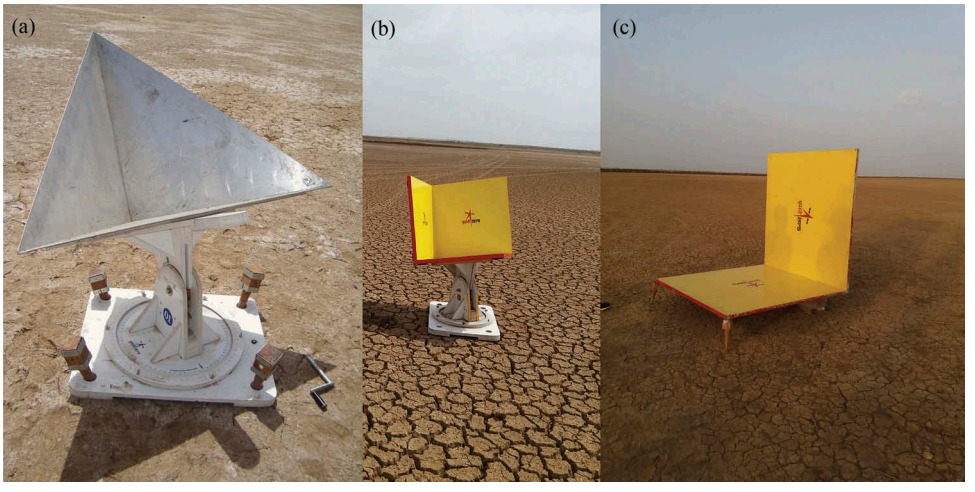

Figure 2. Types of CRs used in the study: (*a*) triangular trihedral, (b) square trihedral, and (c) dihedral.

Table 3. Details of CR used in the study.

CR type	Maximum theoretical RCS	Leg length (m)	RCS (dB m^2)
Triangular trihedral	$\sigma_T = \frac{4\pi a^4}{3\lambda^2}$	0.9	29.491
Square trihedral	$\sigma_T = \frac{12\pi a^4}{\lambda^2}$	0.6	31.921
Dihedral	$\sigma_T = \frac{8\pi a^4}{\lambda^2}$	1.2	42.202

(inner leg length of 1.2 m) used in this study for the radiometric calibration stability assessment of RISAT-1 data. Table 3 shows the detail of the CRs used in this study.

3. Methodology

In the present study, point targets (CRs) array has been used for the radiometric calibration stability assessment of RISAT-1 data. Different types of CRs viz. triangular trihedral, square trihedral, and dihedral were deployed by the calibration team at Desalpar, Rann of Kutch site in India, synchronous to satellite pass for calibration of FRS-1 and MRS mode data. All the CRs were configured as per the calculated parameters with respect to satellite parameters, and their global positioning system co-ordinates were also recorded. Sufficient care was taken while setting up the CR, so that accurate azimuthal as well as elevation angle could be obtained. Utilizing precise levels and compasses, an alignment accuracy of 0.5° for both azimuth and elevation could be achieved. Mobile phones and other metallic objects were kept at far-off distance to avoid any disturbances. Because of large availability of land parcel within the site, it was possible to maintain sufficiently high distance between CRs. Minimum 600 m distance was kept between two nearby CRs in both *x* and *y* direction which is nearly 25 pixels for MRS mode data and 200 pixels for FRS-1 mode data. This will be an advantage while processing the image, as no CR will affect each other's response and overlapping of side lobes can be avoided. After deploying the series of standard angle reflectors with known

scattering cross-section on the ground calibration field synchronous to satellite pass, single look complex (SLC) data of FRS and multi-look, ground range detected product (GRD) of MRS were analysed. It has already been shown by various researchers in the past that the point targets with known scattering cross-section can be used to establish the relation between output signal and the backscattering coefficient. Point targets (CR) were located in the generated intensity images, and the integral method was applied to derive the calibration constant. Referring to Ulander (1991), the theoretical scattering cross-section of the standard angle reflectors (σ_{ref}) to the clutter corrected point target energy (ε_{p}) through the RISAT-1 image of the calibration field was related to the calibration constant (K) as

$$K = \frac{\varepsilon_{\text{p}}}{\sigma_{\text{ref}} \sin\theta}, \tag{1}$$

where, ε_{p} is the clutter-corrected point target energy; σ_{ref} is the theoretical radar cross-section (RCS) of the CR; $\boldsymbol{\theta}$ is the incidence angle of the target. The average measured values (K_{avg}) corresponding to the point targets has been reported as the final measurement result of the calibration for each date and is calculated as

$$K_{\text{avg}} = \frac{1}{N} \sum_{i=1}^{N} K_i, \tag{2}$$

where, N is the number of point targets used and K_i is the measured calibration constant corresponding to point target i.

The key step in measuring the calibration constant is energy associated with point target. There are several methods for deriving the calibration constant K from point targets, including (Woode, Desnos, and Jackson 1992) (i) the peak estimation method and (ii) the integral method applied to pixel values. In this work we followed the integral method which was first proposed by Gray et al. (1990). To determine average clutter intensity, four areas of size 8 ×8 pixels in range and azimuth direction around the point target are selected in such a way that they exclude pixels having influence of point target or any other point target responses (Figure 3). Then, average clutter intensity is calculated and converted into energy by using pixel area. Similarly, point target energy was determined by selecting 8 ×8 cell grid in the range and azimuth direction centred around the point target. 2 ×1 looks in range and azimuth direction, respectively, have been used. Clutter-corrected point target energy (ε_{p}) is determined by subtracting point target energy by average clutter energy.

The large RCS is required to ensure adequate visibility above the surrounding background scatterers, often termed clutter. Due to the clutter and noisy environment on the ground, the clutter contribution adjacent to ground-fixed reference target should be taken into account for the performance estimation. One measure of visibility is the target signal-to-clutter ratio (SCR) and is estimated in the study as follows:

$$\text{SCR} = \frac{\sigma_{\text{p}}}{\sigma_0 A_{\text{res}}}, \tag{3}$$

where, σ_{p} is the backscattered energy of a reference point target, σ_0 is the mean backscattered energy of the clutter, and A_{res} represents the area of the resolution cell (Zénere 2012).

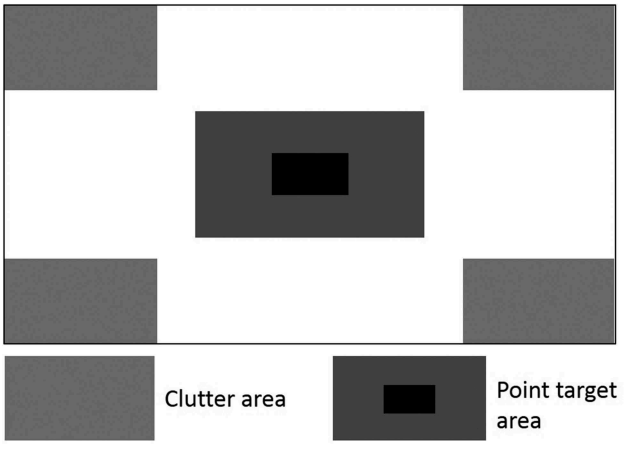

Figure 3. Arrangement of point target and clutter window used in the integral method.

The summary of the steps adopted for the radiometric calibration stability assessment of the FRS-1 and MRS intensity data is shown in Figure 4. For near-range and far-range calibration stability assessment, the methodology adopted by Chapman, Siqueira, and Freeman (2002) has been used.

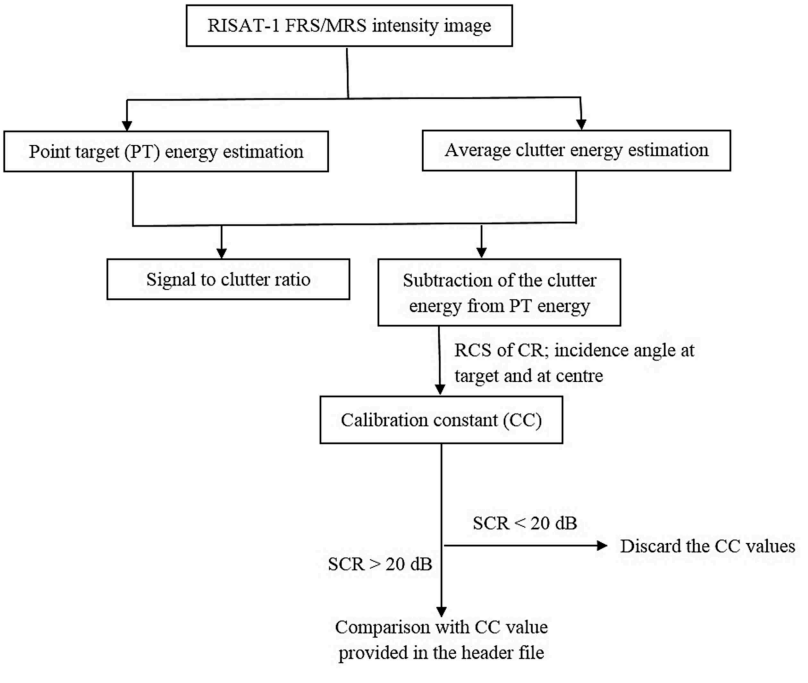

Figure 4. Flow chart of the methodology adopted in the study.

4. Results and discussion

In order to assess the radiometric calibration stability of RISAT-1 SAR sensor, standard point targets of various types (triangular trihedral, square trihedral, and dihedral) with known RCS are deployed prior to satellite overpass with precise azimuth and elevation angles in Desalpar, Rann of Kutch Cal Val site in India. The deployed reflector responses in RISAT-1 SAR images were analysed to derive radiometric parameters of the data and compute the necessary calibration parameters. Tables 4 and 5 show the number of CRs deployed at various sites for different dates for FRS-1 and MRS respectively.

The responses of the deployed CRs at Desalpar, Rann of Kutch site, in RISAT-1 FRS-1 and MRS intensity images are shown in Figures 5–10.

Impulse response functions (IRFs) of the corresponding CRs deployed on 10 March 2016 image are shown in Figure 9 for triangular trihedral and dihedral only. Dihedral corner reflector (CR9) is showing very poor IRF (main lobe is almost flat) as compared to the response of triangular trihedral CRs as can be seen in Figure 9. The reason can

Table 4. Number of CRs deployed for FRS-1 mode.

Date	Beam no.	Polarization	Number of CRs deployed
22 January 2016	66	RH, RV	8 Triangular trihedral
15 February 2016	87		8 Triangular trihedral, 3 square trihedral, and 1 dihedral
10 March 2016	107		8 Triangular trihedral and 1 dihedral
11 March 2016	87		8 Triangular trihedral and 1 dihedral

Table 5. Number of CRs deployed for MRS mode.

Date	Beam no.	Polarization	Number and type of CR deployed
14 February 2016	87–97	HH	8 Triangular trihedral, 3 square trihedral, and 1 dihedral
10 March 2016	87–97	HH	8 Triangular trihedral and 1 dihedral

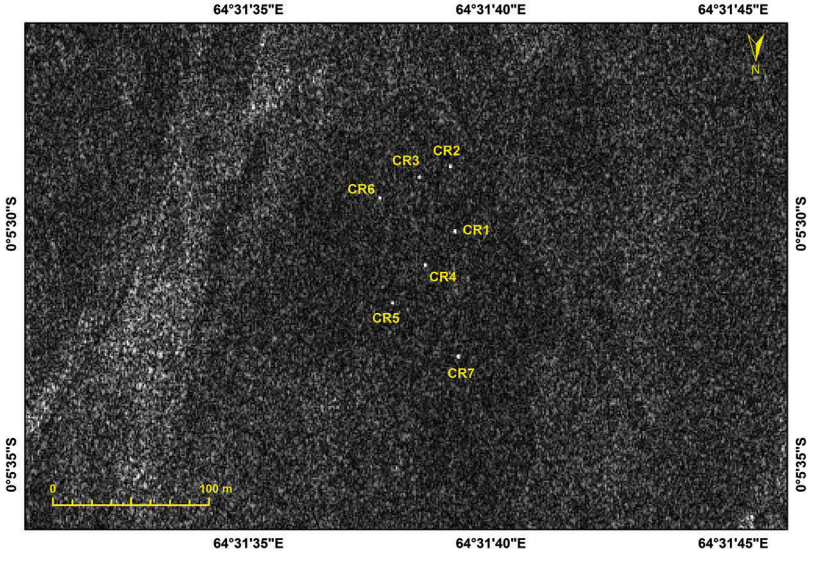

Figure 5. Response of CRs as seen in 22 January 2016, FRS-1 image.

be attributed to the improper alignment of CR9 with respect to satellite parameters as its signal response is very much sensitive to errors in alignment. The error in the orientation of the reflector considerably reduced the backscatter of the reflector's resolution cell, resulting in the absence of the bright target in the image. However, good response of dihedral, square trihedral, and triangular trihedral CRs in both MRS (14 February 2016, HH) and FRS-1 (15 February 2016, RH) images is observed, as is evident from Figures 6 and 7 (bright target response). The comparative analysis of various types of standard point targets (dihedral, square trihedral, and triangular trihedral) is illustrated in Figure 7 and Table 6. It shows the comparison of 3 dB width (range and azimuth) calculated using IRF for various types of CRs for 15

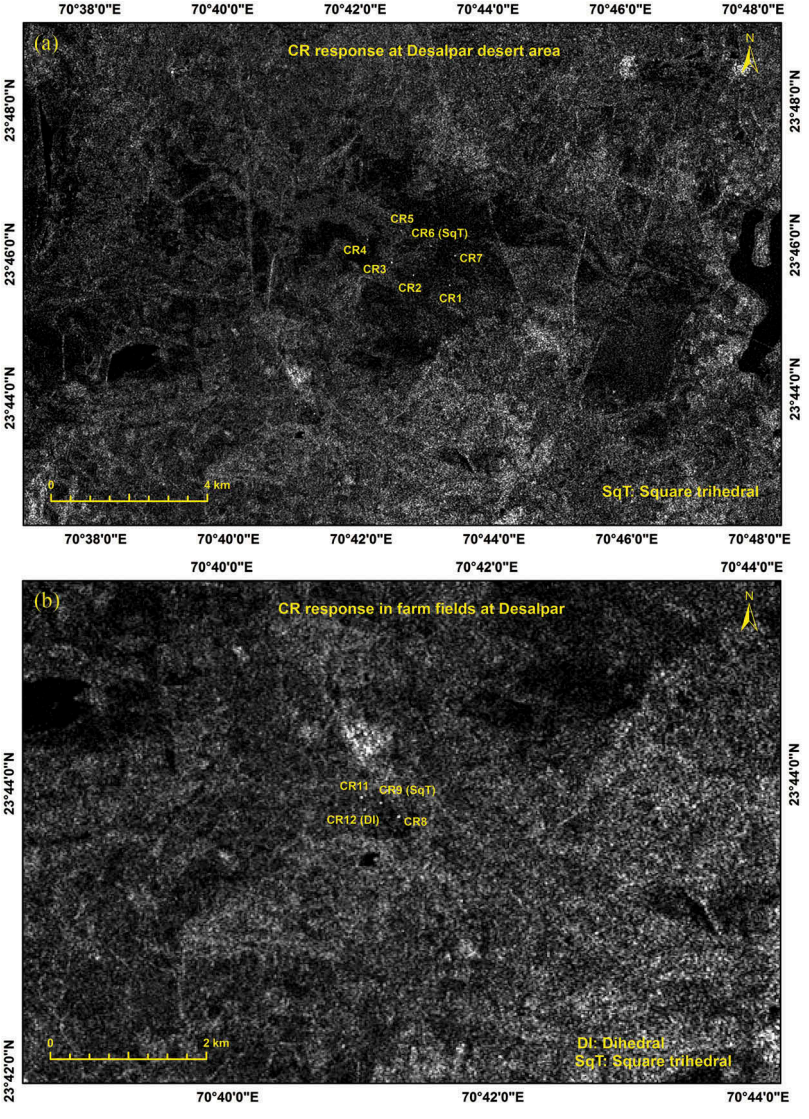

Figure 6. 14 February 2016, MRS image: (a) response of CRs at Desalpar desert area as seen in the image and (b) response of CRs in farm fields at Desalpar as seen in the image.

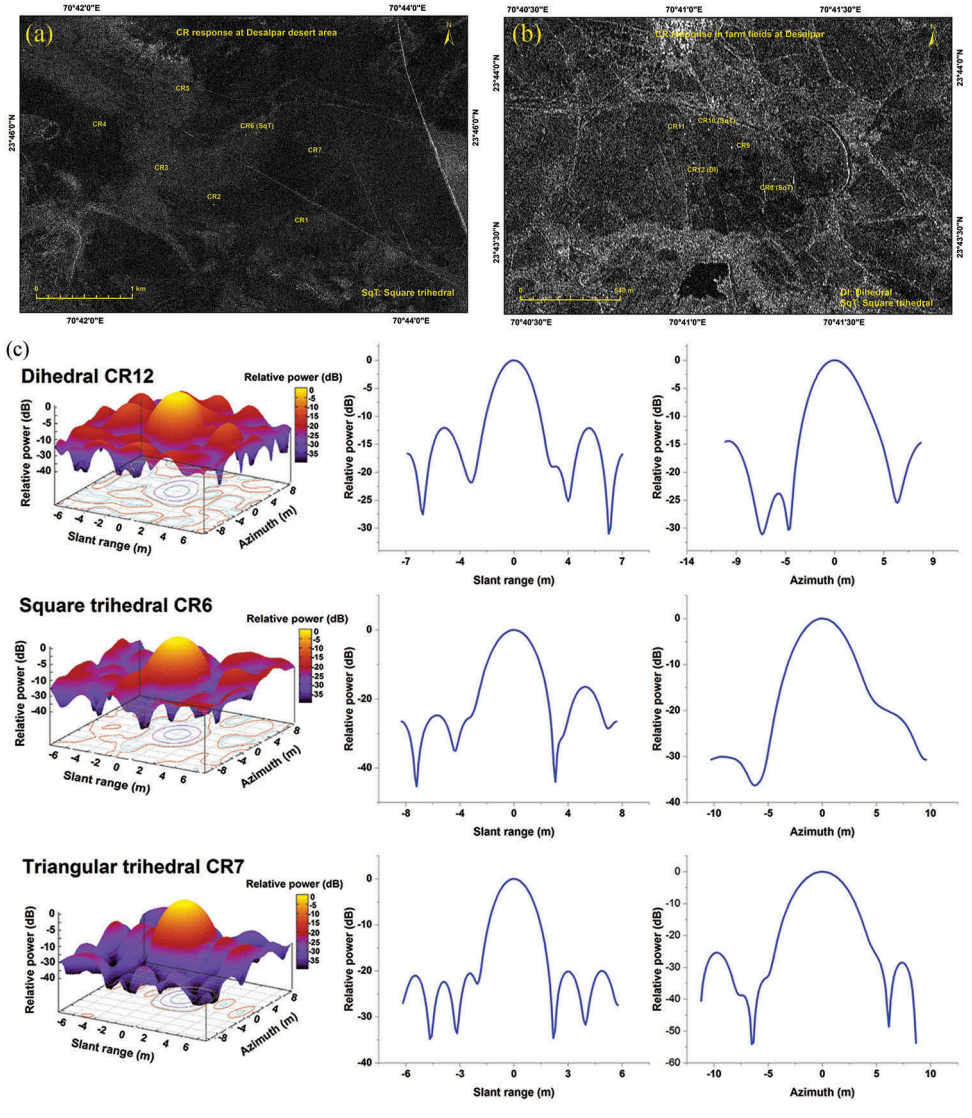

Figure 7. 15 February 2016, FRS-1 (RH polarization, incidence angle 32°) image: (a) response of CRs at Desalpar desert area as seen in the image, (b) response of CRs in farm fields at Desalpar as seen in the image, and (c) IRF of different types of corner reflectors.

Table 6. Comparative study of various types of CR.

		Range resolution (m)	Azimuth resolution (m)	Difference between estimated and specified value (m)	
		Specified (m): 2.34	Specified (m): 3.33		
Polarization	Type of CR	Estimated (m)	Estimated (m)	Range	Azimuth
RH	Dihedral	2.04	3.84	0.30	0.51
	Square trihedral	2.18	3.30	0.16	0.03
	Triangular trihedral	2.10	3.11	0.24	0.22
RV	Dihedral	1.95	3.3	0.39	0.03
	Square trihedral	1.91	3.14	0.43	0.19
	Triangular trihedral	2.09	3.66	0.25	0.33

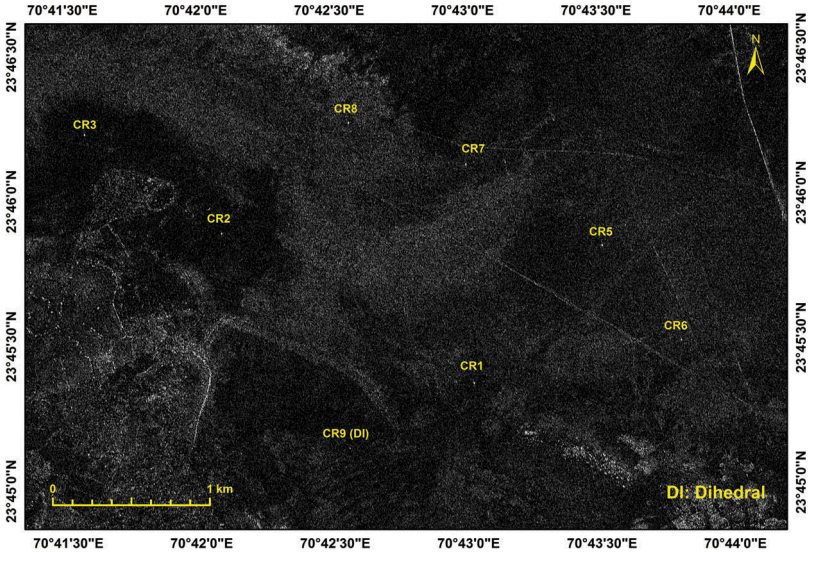

Figure 8. Response of CRs as seen in 10 March 2016, FRS-1 (RV polarization) (all are triangular trihedral CRs except CR9).

February 2016, FRS-1, RH, and RV polarization data. The estimated range and azimuth resolutions are found to be matching well with the corresponding values provided in the header file.

The IRF corresponding to one of the square trihedral (CR8 with size 60 cm) is shown in Figure 11 (a–c)for 14 February 2016 MRS mode HH polarization data and for 15 February 2016 FRS-1 mode RH and RV polarization data, respectively. Peak-to-side-lobe ratio for both range and azimuth is found to be higher for RH and RV polarization as compared to its values in the case of HH polarization. Point target energy and clutter intensity corresponding to CR8 for different dates are shown in Table 7.

SCR was computed for each deployed CR, and it is used as a quality check parameter. Only those results were considered as reliable, where SCR was found to be greater than 20 dB. Figure 12(a) and 12(b) shows the estimated calibration constant for each deployed CR along with the SCR values for MRS mode HH polarization data of 14 February and 10 March 2016, respectively. The difference between estimated and provided calibration constant for FRS-1 mode data of different beams and having different modes and polarizations along with average SCR value is shown in Table 8.

The difference for all the dates for both FRS-1 and MRS mode was found to be within 2 dB as per the defined radiometric calibration specification for point target for RISAT-1 mission (SAC 2015). For the same beam (no. 87) for FRS-1 mode data, results of the analysis show consistency for the estimated calibration constant of different dates (15 February and 11 March 2016). For RH polarization of FRS-1 having beam no. 87, the estimated average calibration constant was found to be 69.98 and 72.77 dB for 15 February and 10 March 2016 data, respectively, whereas, for the same beam having RV polarization the estimated values are 66.60 and 69.36 dB, respectively.

Central Amazon Rainforest (latitude: 6.486717° N, longitude: 65.590916° E) was selected to evaluate stability of calibration in the same scene as this site is considered to be flat

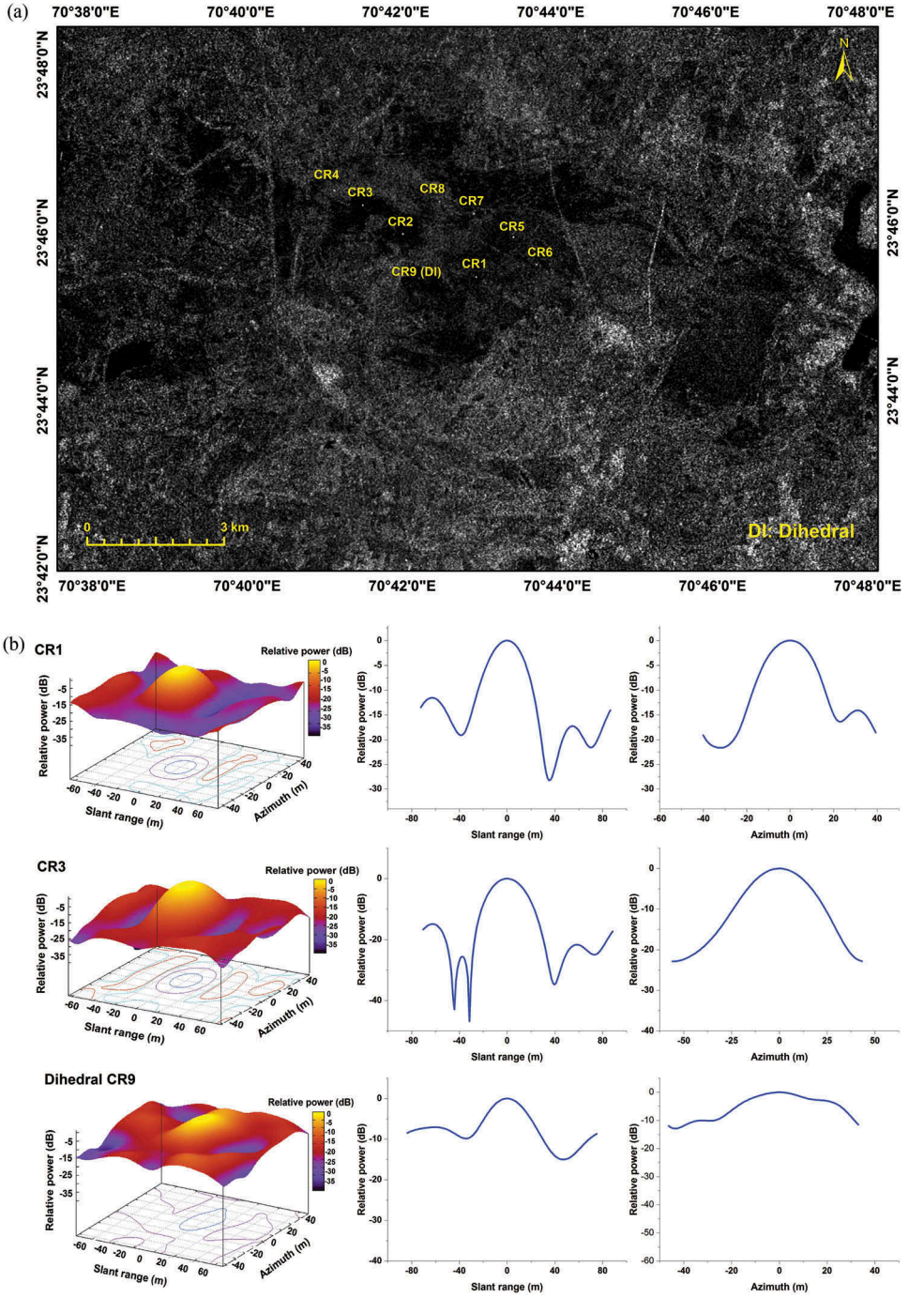

Figure 9. 10 March 2016, MRS image (HH polarization, incidence angle 36°): (a) response of CRs as seen in the image (all are triangular trihedral CRs except CR9) and (b) IRF of the CRs.

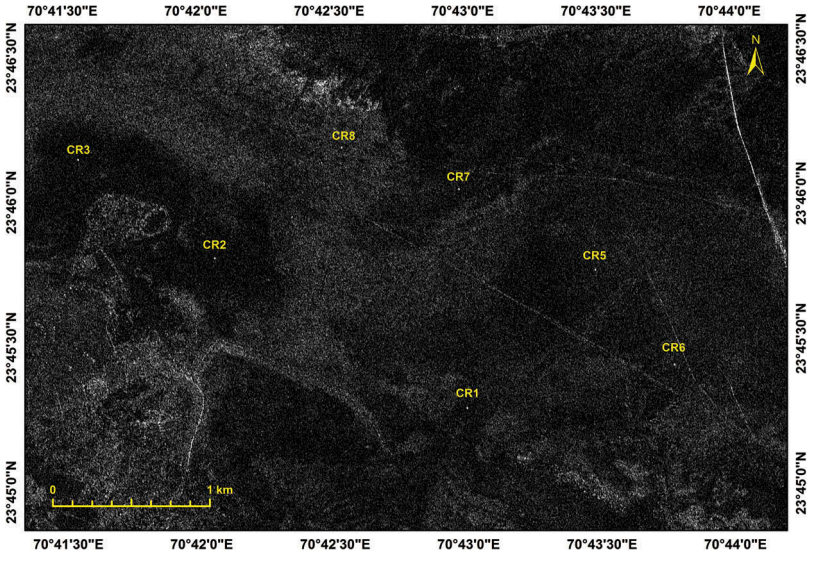

Figure 10. Response of CRs at Desalpar Cal Val site (same area as shown in Figure 9) as seen in 11 March 2016 FRS-1 image (all are triangular trihedral CRs).

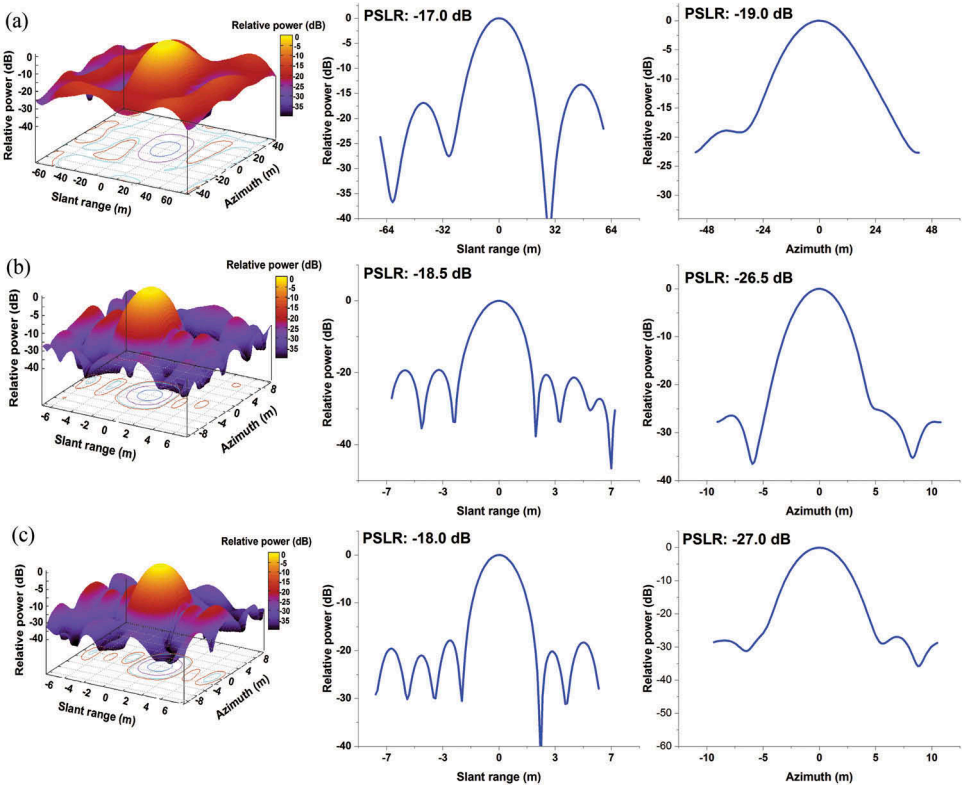

Figure 11. IRF of square trihedral corner reflector (CR8) observed for: (a) 14 February 2016, MRS HH, (b) 15 February 2016, FRS-1 RH,and(c)15 February 2016, FRS-1 RV.

Table 7. Results of point target analysis of square trihedral CR.

Date of pass	Point target energy including clutter (dB)	Average clutter intensity (dB)	Incidence angle at point target (°)	Polarization mode
14 February 2016	83.54	59.67	35.50	MRS, HH, GRD
15 February 2016	92.25	57.42	32.43	FRS, RH, SLC
15 February 2016	88.68	57.64	32.43	FRS, RV, SLC

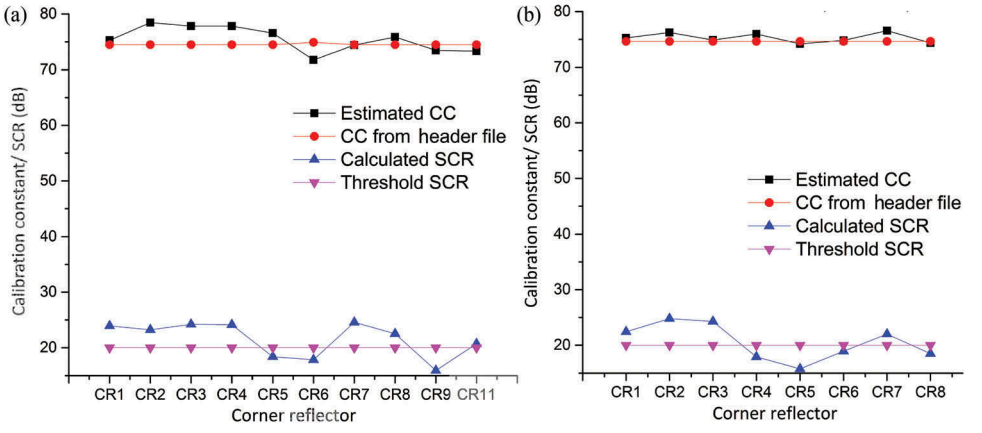

Figure 12. Estimated calibration constant and SCR for: (a) 14 February and (b) 10 March 2016 GRD product of MRS mode data with HH polarization.

Table 8. Estimated calibration constant (CC) and SCR for FRS-1 mode.

Date	Beam no.	Mode	Polarization	CC provided with data (dB)	Estimated CC (dB) Mean	Standard deviation	Difference with mean of estimated CC (dB)	SCR (dB)
22 January 2016	66	SLC	RH	71.832	70.015	0.636	1.816	26.32
	66	SLC	RV	66.597	66.083	0.854	0.513	26.04
15 February 2016	87	SLC	RH	70.645	69.989	0.529	0.655	32.83
	87	SLC	RV	67.478	66.601	0.260	0.876	31.93
10 March 2016	107	SLC	RH	74.222	72.774	0.382	1.447	38.44
	107	SLC	RV	71.019	69.365	0.521	1.653	37.68
	107	GRD	RH	71.262	71.695	0.379	−0.433	38.98
	107	GRD	RV	68.058	67.774	0.521	0.283	37.39
11 March 2016	87	SLC	RH	70.582	69.918	0.434	0.663	34.39
	87	SLC	RV	67.416	66.287	0.651	1.128	33.62
	87	GRD	RH	67.623	69.661	0.412	−2.038	36.74
	87	GRD	RV	64.456	66.008	0.600	−1.552	35.40

terrain and uniform in nature. Assuming a constant γ_0 (gamma-nought), which is defined as the normalized RCS divided by the cosine of the incidence angle, for the rainforest over the incidence angles implies that a pixel observed at far-range incidence angle and near-range incidence angle in same scene should have the same γ_0 value in both sides. Three scenes of MRS mode RISAT-1 data of 16 January 2014, 23 February 2014, and 17 February 2015 were used for the analysis. The incidence angle variation is shown in Table 9. The nominal value of γ_0 for HH is −6.5 dB and nominal γ_0 for HV is −12.5 dB (Schwerdt et al. 2016; Hawkins

Table 9. Near-range and far-range calibration results.

Date	Range	Mean incidence angle (°)	Estimated γ_0 (dB)		Near- to far-range difference (dB)		Difference from reported γ_0 (dB)	
			HV	HH	HV	HH	HV	HH
16 January 2014	Near range	25.82	−12.3	−6.0	0.1	0.1	0.2	0.5
	Mid range	30.66	−12.3	−5.9			0.2	0.6
	Far range	34.92	−12.4	−5.9			0.1	0.6
23 February 2014	Near range	14.70	−11.7	−5.5	0.0	0.2	0.8	1.0
	Mid range	20.19	−11.7	−5.7			0.8	0.8
	Far range	25.07	−11.7	−5.5			0.8	1.0
17 February 2015	Near range	46.81	−11.8	−5.9	0.3	0.2	0.7	0.6
	Mid range	49.91	−11.8	−5.7			0.7	0.8
	Far range	52.90	−11.5	−5.8			1.0	0.7

et al. 2000). Four different regions (at different azimuth but same range) each at near range, centre of the scene, and far range were evaluated for each scene, and γ_0 was estimated. Average value of γ_0 was reported for near range, centre, and far range for same scene. The results of the analysis are shown in Table 9.

It can be seen from Table 9 that as we move from near range to far range the γ_0 value remains nearly constant with the difference in the range of 0.1–0.2 dB for HH polarization and 0.1–0.3 dB for HV polarization. However, the difference between the γ_0 value estimated and reported in the literature (Schwerdt et al. 2016; Hawkins et al. 2000) was found to be within the mission specification (1 dB for relative calibration).

4.1. *Uncertainty analysis*

The theoretical value of RCS of CR tends to reduce due to mechanical imperfections which in turn will have an impact on the calibration results. The factors that can act to reduce the RCS of a CR at boresight compared to the theoretical value are misalignment of the reflector, inter-plate orthogonality, plate curvature, size deviation, and surface irregularities. The reduction in RCS due to various factors is described in Zink and Kietzmann (1995), Ulander et al. (1991), and Döring, Schwerdt, and Bauer (2007). For uncertainty analysis in this study, the manufacturing tolerance specifications of the CRs (Table 10) were used. From these values, the RCS reductions have been computed to achieve the actual radar cross-section of each reflector.

The RCS error-budget due to the abovementioned factors (using the manufacturing tolerance specifications) was calculated for each type of CRs. The total calibration uncertainty was then estimated by calculating the root mean square error (RMSE) using the following equation:

Table 10. Tolerance specifications of CR used.

Reflector type	Inner leg length of CR (m)	Size tolerance (mm)	Inter-plate orthogonality	Surface flatness	Surface irregularity RMSE
Triangular trihedral	0.9	± 0.5	Better than 0.20°	Less than 0.4 mm	Less than 0.2 mm
Square trihedral	0.6	± 1			
Dihedral	1.2	± 2			

$$\text{RMSE} = \sqrt{\frac{\sigma_1^2 + \sigma_2^2 + \sigma_3^2 + \sigma_4^2 + \sigma_5^2}{5}}, \tag{4}$$

where, $\sigma_i i$ =1,2,3,4,5 are the estimated error due to misalignment of the reflector, inter-plate orthogonality, plate curvature, size deviation, and surface irregularities, respectively. The total RMSE for triangular trihedral and square trihedral was found to be 0.15 and 0.45 dBm^2, respectively.

5. Conclusions

This study presents the recent results of the absolute radiometric calibration of RISAT-1 FRS-1 and MRS mode data using different types and sizes of point targets in a desert environment site in Desalpar, Rann of Kutch, western India. In all, six calibration campaigns data (four data for FRS-1 and two data for MRS) spanning from 22 January 2016 to 11 March 2016 were used for the study. The results obtained show that the difference between the estimated average calibration constants for FRS-1 and MRS mode intensity data with the provided value was found to be within 2 dB which meets the defined absolute radiometric accuracy specification for RISAT-1 mission. Near-range and far-range calibration stability assessments were done using distributed target. The results of this calibration stability assessment analysis indicate that as we move from near range to far range, the γ_0 value remains nearly constant with the difference in the range of 0.1–0.2 dB for HH polarization and 0.1–0.3 dB for HV polarization.

SCR was also computed for each deployed CR, and it was found that for the study site, average SCR is greater than 20 dB which is prime requirement for the precisely calibrated results. Effect of the varying target and clutter window size on the estimated calibration constant showed that the results do not show much variation when target and clutter of different window sizes were used for the computation of background corrected point target energy. This shows that the background of Desalpar Cal Val site is uniform and homogeneous indicating that it can be used as an operational SAR calibration site for C-band, whereas, for other frequencies, the suitability of this site needs to be checked.

Acknowledgements

Authors express their sincere gratitude to Shri Tapan Misra, Director, Space Applications Centre, Ahmedabad, and Dr. Rajkumar, Deputy Director, EPSA, for their guidance and support to carry out this activity. Authors are grateful to Director, Institute of Technology, Nirma University, HOD, Civil Engineering Department, Nirma University, and Principal, M.G. Science Institute, Ahmedabad, for their institutional support for carrying out this activity. Authors also thankfully acknowledge the cooperation and technical help received from Shri D. B. Dave, Dr. Kartikeyan, Shri Ramanujam, Shri Amit Shukla, and Shri Raghav Mehra for this activity. The help and support rendered by Shri Ganuba, Shri Digvijay, and Shri Parvat during the deployment of CRs at Desalpar and their navigational guidance of the local area were of utmost importance for the successful calibration campaigns.

Disclosure statement

No potential conflict of interest was reported by the authors.

References

Chapman, B., P. Siqueira, and A. Freeman. 2002. "The JERS Amazon Multi-Season Mapping Study (JAMMS): Observation Strategies and Data Characteristics." *International Journal of Remote Sensing* 23 (7): 1427–1446. doi:10.1080/01431160110092966.

Corr, D. 1982. *SAR580 Campaign: Data Analysis in Support of Calibration*. Final. Rep, Farnborough, UK: Systems Designers .

Cote, S. J., S. K. Srivastava, R. K. Hawkins, and P. Le Dante (2007, October). RADARSAT Calibration Operations at the Canadian Space Agency: Maintaining RADARSAT-1 Performance and Preparations for RADARSAT-2. In *IET International Conference* on *Radar Systems, 2007*, 15th – 18th October, 2007, Edinburgh, UK, pp. 1–5.

Dobson, M. C., F. T. Ulaby, D. R. Brunfeldt, and D. N. Held. 1986. "External Calibration of SIR-B Imagery with Area-Extended and Point Targets." *IEEE Transactions on Geoscience and Remote Sensing*, no. 4: 453–461. doi:10.1109/TGRS.1986.289659.

Döring, B., M. Schwerdt, and R. Bauer, 2007. TerraSAR-X Calibration Ground Equipment. In *Wave Propagation in Communication, Microwaves Systems and Navigation-2007 (WFMN07)* July, 2007, Chemnitz, Germany, pp. 86–90.

European Space Agency (ESA) "Sentinel-1 Radiometric Calibration of Products", Issue 1 Rev 0, 21 May 2015, Report no. ESA-EOPG-CSCOP-TN-0002. Available online at https://sentinel.esa.int/web/sentinel/user-guides/sentinel-1-sar,Sentinel1Radiometric calibration of Products (Last accessed on 27 October 2016).

Freeman. "SIRC/X Data Quality and Calibration Results." *IEEE Transactions on Geoscience and Remote Sensing*. 33(4);848–857; Jul 1995. Doi:10.1109/36.406671.

Freeman, A. 1992. "SAR Calibration: An Overview." *IEEE Transactions on Geoscience and Remote Sensing* 30 (6): 1107–1121. doi:10.1109/36.193786.

Gray, A. L., P. W. Vachon, C. E. Livingstone, and T. I. Lukowski. 1990. "Synthetic Aperture Radar Calibration Using Reference Reflectors." *IEEE Transactions on Geoscience and Remote Sensing* 28 (3): 374–383. doi:10.1109/36.54363.

Gupta, M., B. Kartikeyan, and S. Chowdhury. 2014. "An Approach to Evaluate and Monitor RISAT-1 SAR from Level-0 Raw Data." *International Journal of Remote Sensing* 35 (16): 6043–6059. doi:10.1080/01431161.2014.943323.

Hawkins, R., E. Attema, R. Crapolicchio, P. Lecomte, J. Closa, P. J. Meadows, and S. K. Srivastava, 2000, March. Stability of Amazon Backscatter at C-Band: Space-borne Results from ERS-1/2 and RADARSAT-1. In *SAR workshop: CEOS Committee on Earth Observation Satellites*, 26-29 October 1999, Toulouse, French (Vol. 450, p. 99).

Misra, T., and A. S. Kirankumar, 2014. RISAT-1: Configuration and Performance Evaluation. In *General Assembly and Scientific Symposium (URSI GASS), 2014 XXXIth URSI*, Beijing, 16-23 August 2014, pp. 1–4.

Misra, T., S. S. Rana, N. M. Desai, D. B. Dave, A. R. K. Rajeevjyoti, C. V. N. Rao, B. V. Bakori, R. Neelakantan, and J. G. Vachchani. 2013. "Synthetic Aperture Radar Payload On-Board RISAT-1: Configuration, Technology and Performance." *Current Science* 104 (4): 446.

SAC (Space Applications Centre, ISRO), 2015, RISAT-1 Data Products Formats. Available online at http://www.nrsc.gov.in/sites/all/pdf/risat-1brochurev4.pdf accessed on 27 April 2016).

Schmidt, K., M. Schwerdt, N. Tous Ramon, G. Castellanos Alfonzo, and M. Zink, 2015. Sentinel-1A Calibration Support during Routine Operation Using Innovative Point Targets. *Wave Propagation in Communication, Microwaves Systems and Navigation-2007 (WFMN07)*July, 2007, Chemnitz, Germany. Available online at http://elib.dlr.de/95389 (accessed on 07 November 2016)

Schwerdt, M., K. Schmidt, N. T. Ramon, G. C. Alfonzo, B. J. Döring, M. Zink, and P. Prats-Iraola. 2016. "Independent Verification of the Sentinel-1A System Calibration." *IEEE Journal of Selected Topics in Applied Earth Observations and Remote Sensing* 9 (3): 994–1007. doi:10.1109/JSTARS.2015.2449239.

Shimada, M. 2015. "Calibration and Validation of PALSAR2." *Proceeding of IGARSS'15*, Milan, Italy, 26–31 July 2015. doi: 10.1109/IGARSS.2015.7326730

Shimada, M., O. Isoguchi, T. Tadono, and K. Isono. 2009. "PALSAR Radiometric and Geometric Calibration." *IEEE Trans. Geosci. Remote Sens.* 47 (12, Dec): 3915–3932. doi:10.1109/TGRS.2009.2023909.

Srivastava, S. K., N. W. Shepherd, T. I. Lukowski, and R. K. Hawkins. 1996. "Plans for RADARSAT Image Data Calibration." *Advances in Space Research* 17 (1): 89–96. doi:10.1016/0273-1177(95)00453-L.

Srivastava, S. K., P. Le Dantec, R. K. Hawkins, B. T. Banik, R. Gray, K. Murnaghan, G. Guertin, and N. Shepherd. 2003. "RADARSAT-1 Image Quality and calibration—Continuing Success in Extended Mission." *Advances in Space Research* 32 (11): 2295–2304. doi:10.1016/S0273-1177(03)90557-6.

Srivastava, S. K., R. K. Hawkins, B. T. Banik, M. Adamovic, R. Gray, K. Murnaghan, T. I. Lukowski, and W. C. Jefferies. 2001. "RADARSAT-1 Image Quality and Calibration—A Continuing Success." *Advances in Space Research* 28 (1): 99–108. doi:10.1016/S0273-1177(01)00305-2.

Touzi, R. K. 2012. "Hawkins and S. Cote, "On the Use of Transponder for High Precision Assessment & Calibration of Polarimetric Radarsat2"." *Ieee Tgrs* 51 (1, January): 487–503.

Ulander, I. M. H. 1991. "Accuracy of Using Point Targets for SAR Calibration." *IEEE Transactions on Aerospace and Electronic Systems* 27 (1): 139–148. doi:10.1109/7.68156.

Ulander, L. M., R. K. Hawkins, C. E. Livingstone, and T. I. Lukowski. 1991. "Absolute Radiometric Calibration of the CCRS SAR." *IEEE Transactions on Geoscience and Remote Sensing* 29 (6): 922–933. doi:10.1109/36.101371.

Woode, A. D., Y. L. Desnos, and H. Jackson. 1992. "The Development and First Results from the ESTEC ERS-1 Active Radar Calibration Unit." *IEEE Transactions on Geoscience and Remote Sensing* 30 (6): 1122–1130. doi:10.1109/36.193787.

Zénere, M. P., 2012. SAR Image Quality Assessment. Available online at http://aulavirtual.ig.conae.gov.ar/moodle/pluginfile.php/513/mod_page/content/78/MirkoPanozzoZenere.pdf on 10 November 2016.

Zink, M., and H. Kietzmann, 1995. Next Generation SAR-External Calibration. German Aerospace Center (DLR). Technical report 95-41. Available online at http://elib.dlr.de/33370 (accessed on 07 November 2016)